Suppression of DNA-damage checkpoint signaling by Rsk-mediated phosphorylation of Mre11

Chen Chen, Liguo Zhang, Nai-Jia Huang, Bofu Huang, and Sally Kornbluth[1]

Department of Pharmacology and Cancer Biology, Duke University School of Medicine, Durham, NC 27710

Edited by Tony Hunter, The Salk Institute for Biological Studies, La Jolla, CA, and approved November 12, 2013 (received for review April 9, 2013)

Ataxia telangiectasia mutant (ATM) is an S/T-Q–directed kinase that is critical for the cellular response to double-stranded breaks (DSBs) in DNA. Following DNA damage, ATM is activated and recruited by the MRN protein complex [meiotic recombination 11 (Mre11)/DNA repair protein Rad50/Nijmegen breakage syndrome 1 proteins] to sites of DNA damage where ATM phosphorylates multiple substrates to trigger cell-cycle arrest. In cancer cells, this regulation may be faulty, and cell division may proceed even in the presence of damaged DNA. We show here that the ribosomal s6 kinase (Rsk), often elevated in cancers, can suppress DSB-induced ATM activation in both *Xenopus* egg extracts and human tumor cell lines. In analyzing each step in ATM activation, we have found that Rsk targets loading of MRN complex components onto DNA at DSB sites. Rsk can phosphorylate the Mre11 protein directly at S676 both in vitro and in intact cells and thereby can inhibit the binding of Mre11 to DNA with DSBs. Accordingly, mutation of S676 to Ala can reverse inhibition of the response to DSBs by Rsk. Collectively, these data point to Mre11 as an important locus of Rsk-mediated checkpoint inhibition acting upstream of ATM activation.

dsDNA IP | PMA | SL0101 | γ-H2AX

Cells have evolved multiple pathways signaling DNA damage that trigger DNA repair, cell-cycle arrest and, in the event of irreparable damage, cell death. Among the various forms of DNA damage, double-stranded breaks (DSBs) in DNA, generated by exposure to ionizing radiation and radiomimetic chemicals such as neocarzinostatin (NCS), are the most lethal for cells (1).

DSBs often are repaired by homologous recombination during the S and G2/M phases of the cell cycle, which involves the meiotic recombination 11 (Mre11)/DNA repair protein Rad50/Nijmegen breakage syndrome 1 (Nbs1) (MRN) complex and the ataxia telangiectasia mutated (ATM) kinase (2, 3). The MRN complex first recognizes sites of DNA damage and then promotes binding of ATM to the DSB site. ATM, activated by monomerization and autophosphorylation, phosphorylates downstream proteins including p53, checkpoint kinase 2 (Chk2), and breast cancer 1, early onset (BRCA1) (4-7). These factors then convey the signal to induce cycle arrest, apoptosis, or DNA repair (8). Failure of this process results in genome instability, increasing the risk of cancer, neurodegeneration, and other pathologies (9).

Ribosomal S6 kinase (Rsk), which functions downstream of mitogen-activated protein kinase kinase (MEK) and ERK, is frequently activated in cancer cells (10, 11). Rsk activation can be promoted by multiple signaling pathways in cancer cells, including those triggered by steroids, insulin, EGF, and estrogen (10, 12–15). Additionally, Rsk activation can be triggered by PKC signaling [via the PKC/rapidly accelerated fibrosarcoma (RAF)/mitogen-activated protein kinases (MAPK) pathway], which is activated by phorbol12-myristate13-acetate (PMA) (16, 17). Previous studies have found that Rsk2 is overexpressed in 50% of breast cancers and prostate tumors (18, 19), and Rsk signaling has been implicated in the regulation of survival, anchorage-independent growth, and transformation of breast cancer cells in culture (20). Rsk-specific inhibition (with BI-D1870 or SL0101) significantly reduced proliferation of MCF7, PC3, or LnCaP cancer cells (18, 19). Rsk also inhibits apoptosis in PC3 prostate cancer cells (21).

A hallmark of cancer cells is their ability to override cell-cycle checkpoints, including the DSB checkpoint, which arrests the cell cycle to allow adequate time for damage repair. Previous studies have implicated the MAPK pathway in inhibition of DNA-damage signaling: PKC suppresses DSB-induced G2/M checkpoint signaling following ionizing radiation via activation of ERK1/2 (22); activation of RAF kinase, leading to activation of MEK/ERK/Rsk, also can suppress G2/M checkpoint signaling (23).

Given its prominent role in multiple cancers, the MAPK pathway is an attractive therapeutic target. Indeed, treatment of melanoma using the RAF inhibitor vemurafenib has shown some clinical success, as has treatment of nonsmall cell lung carcinoma with MEK inhibitors (24). However, targeting components at the apex of a signaling pathway may induce side effects caused by the plethora of downstream effectors (25, 26). As a terminal kinase in the MAPK pathway, Rsk may avoid these complications as a potential target. Thus, there has been interest in targeting Rsk for cancers with notable Rsk elevation (e.g., prostate cancers) (27). Several Rsk-specific inhibitors have been described, including SL0101 and BI-D1870 (18, 28, 29). Whether these or derivative drugs will be clinically successful remains unclear. However, if Rsk inhibition can reinstate DSB-induced checkpoint function, then combination therapy of Rsk inhibitors with DNA-damaging agents may be effective in inducing tumor cell arrest or death.

The precise mechanism underlying checkpoint inhibition downstream of MEK/ERK/Rsk signaling is not yet clear. One recent paper has shown that, after doxorubicin-induced DNA damage (both DSB and ssDNA breaks), Rsk can silence the G2/M checkpoint by phosphorylating (and inhibiting) the Chk1 kinase on S280 (the same site that can be targeted by protein kinase B/Akt kinase) (30). However, another group has reported that phosphorylation of this site on Chk1 enhanced its ability to enforce the checkpoint by promoting its nuclear translocation (31).

We show here that Rsk signaling silences the DSB-induced G2/M checkpoint by preventing activation of the ATM kinase. Specifically, we have found that Rsk targets the Mre11 component of the MRN complex by phosphorylating S676, thereby preventing Mre11 binding to DNA. Mutation of S676 restored ATM activation, even in the face of high Rsk activity, and rendered

Significance

We have identified a pathway that links MAPK/ribosomal s6 kinase (Rsk) signaling to the inhibition of the response to a double-stranded break (DSB) in DNA, potentially explaining radioresistance in tumors with high rapidly accelerated fibrosarcoma (Raf)/MAPK/Rsk activity. The locus of this regulation was identified as meiotic recombination 11, whose phosphorylation by Rsk prevented its DNA binding and consequent activation of the central DSB checkpoint regulator, ataxia telangiectasia mutant.

Author contributions: C.C. and S.K. designed research; C.C., L.Z., N.-J.H., and B.H. performed research; C.C. analyzed data; and C.C. and S.K. wrote the paper.

The authors declare no conflict of interest.

This article is a PNAS Direct Submission.

[1]To whom correspondence should be addressed. E-mail: sally.kornbluth@duke.edu.

This article contains supporting information online at www.pnas.org/lookup/suppl/doi:10.1073/pnas.1306328110/-/DCSupplemental.

cells refractory to the checkpoint-inhibitory effects of Rsk. This finding is consistent with a previous study showing that phosphorylation on Mre11 is mostly inhibitory (32). Taken together, these findings identify a locus of checkpoint regulation by Rsk and support the idea of targeting Rsk for therapeutic benefit.

Results

Prostate Cancer Cells with High Levels of Endogenous Rsk Are Resistant to DSBs. Rsk is highly expressed in many prostate cancer cell lines, including PC3 and LnCaP cells, which appear to be highly dependent on Rsk activity for growth and survival (19). We hypothesized that Rsk might modulate the response of these cells to DNA damage-induced checkpoint function. To evaluate this hypothesis, we analyzed cell-cycle progression after DSB induction in PC3 cells that endogenously express twice the level of Rsk protein found in normal prostate tissue (19). Cells were arrested at G1/S using double thymidine block and 4 h after release were treated with PMA and/or SL0101, followed by NCS to induce DSBs during the G2 phase. After drugs were washed away, cells were incubated in fresh media for 16 h before DNA contents were analyzed. As shown in Fig. 1*A*, cotreatment of cells with SL0101 and NCS resulted in much more robust G2/M arrest than seen with NCS alone. Additionally, after PMA-induced Rsk activation, the DSB-induced G2/M arrest was effectively overridden. We obtained similar results in experiments in which Rsk1/2 were knocked down using siRNA (Fig S1*A*). Taken together, these data suggest that Rsk might inhibit the DSB checkpoint in PC3 prostate cancer cells. To examine this possibility further, we stained PC3 cells for γ-H2AX, a downstream target of ATM. As shown in Fig. 1*B*, PC3 cells treated with SL0101 before NCS treatment displayed greatly increased γH2AX staining. These data strongly suggest that high Rsk activity can suppress ATM-dependent G2/M checkpoint signaling.

Although it has been reported that inhibiting ATM may enhance G2/M accumulation (33), inhibiting ATM decreased the G2/M population in the cell lines we used (Fig S1*B*). This result also is consistent with other published studies (34, 35).

To determine if Rsk is sufficient to confer resistance to DSB-induced G2/M arrest, we overexpressed constitutively active Rsk2 in 293T cells, which have much lower endogenous levels of Rsk than PC3 cells. As shown in Fig. 1*C*, Rsk-expressing cells were considerably less sensitive to DNA damage than control cells. To demonstrate G2/M checkpoint suppression, directly, we synchronized HeLa cells in G1/S phase by double thymidine block and treated them 4 h after release with PMA or SL0101 for 30 min and with NCS for an additional 30 min. Three or five hours later, cells were stained with anti–phospho-Histone H3 (PHH3) antibody. As shown in Fig. S1*C*, NCS significantly reduced the number of pHH3-positive cells by arresting cells in G2 phase. However, PMA treatment greatly increased the pHH3-positive population (particularly at 5 h), suggesting that the G2/M checkpoint had been silenced. This checkpoint inhibition was reversed by cotreatment with SL0101, confirming a role for Rsk in this silencing.

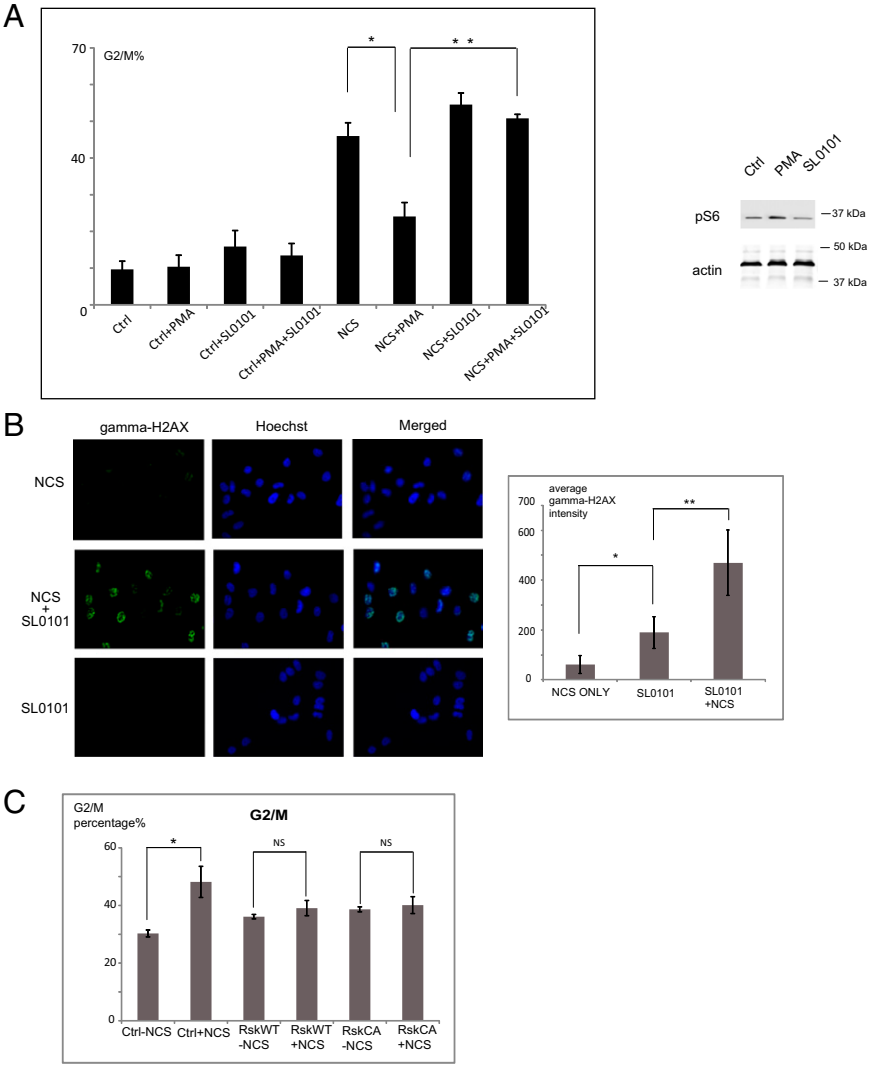

Fig. 1. Rsk suppresses the DSB response in prostate cancer. (*A*) PC3 cells were synchronized in G1/S phase by double thymidine block. Four hours after release, cells were treated with PMA or SL0101 as indicated and then with NCS and were analyzed for DNA content. $n = 3$ experiments. The effectiveness of PMA and SL0101 in modulating Rsk activity was shown by immunoblotting for the Rsk substrate, S6. $*P < 0.01$; $**P < 0.01$. Error bars indicate SD. (*B*) PC3 cells grown on coverslips were treated with SL0101 or DMSO and then with NCS. Fixed cells stained for γH2AX were examined by fluorescent microscopy (20×). The average intensity of γH2ax staining for more than 50 cells from at least seven random fields was quantified with MetaMorph. $*P < 0.01$; $**P < 0.01$. (*C*) 293T cells transfected with FLAG-tagged WT or constitutively active Rsk2 were treated with NCS. DNA profiles of FLAG-positive sorted cells were analyzed to quantify cells in G2/M. $n = 3$ experiments. $*P < 0.05$. Error bars indicate SD. *P* values are derived from the Student *t* test.

Rsk Suppresses the DSB Response by Inhibiting the Activation of ATM. To identify the locus of Rsk action within the DSB-signaling pathway, we assessed the status of the ATM kinase following NCS treatment in cells overexpressing constitutively active Rsk2. We found that after treatment with NCS these cells had reduced ATM phosphorylation at S1981 (a hallmark of ATM activation) but no change in ATM protein levels (Fig. 2*A*). Similarly, PMA treatment markedly decreased ATM autophosphorylation at S1981. However, ATM phosphorylation was restored when cells were treated with both PMA and SL0101 (Fig. S2*A*). To demonstrate further the down-regulation of ATM, we measured phosphorylation of NBS1 at S343, a site known to be targeted by ATM. As expected, phosphorylation of NBS1 was reduced in the presence of PMA, consistent with Rsk-mediated reduction in ATM activity (Fig. S2*B*). Accordingly, siRNA knock down of Rsk in PC3 cells significantly increased ATM autophosphorylation in response to NCS treatment (Fig. 2*B*). ATM autophosphorylation is a very early event in the DSB response, and these data suggest that Rsk acts either at or upstream of ATM. As is consistent with an effect of Rsk signaling on ATM activity, HeLa cells treated with PMA stained more weakly with antibody directed against γH2AX than did untreated cells, and cotreatment with PMA and SL0101 reversed the diminution in γH2AX staining (Fig. 2*C* and Fig. S2*C*). HeLa cells transfected with FLAG-tagged constitutively activated Rsk2 exhibited significantly less γH2AX staining than nontransfected cells after NCS treatment (Fig. 2*D* and Fig. S2*D*). This effect was reversed by treatment with SL0101 (Fig. 2*D* and Fig. S2*D*). Collectively, these data suggest that Rsk signaling suppresses both ATM activation and phosphorylation of its downstream targets, NBS1 and H2AX.

It is worth noting that ATM activation is detected robustly only at the early phases of the DSB response (and thus the effects of Rsk could not be detected later, at 24 h) (Fig. S2*E*). This situation probably reflects checkpoint adaptation or recovery from DNA damage, as is consistent with previous reports (36, 37). However, cells were still phenotypically arrested at 24 h because either (*i*) the remaining ATM activity/DSB response is sufficient to maintain the checkpoint or (*ii*) checkpoint recovery lags behind DSB response recovery because cells require time to resume the cell cycle even though the upstream DNA-damage signals have waned.

The Moloney Sarcoma Oncogene/MAPK/Rsk Pathway Inhibits Binding of the MRN Complex to dsDNA. To identify the direct targets of Rsk responsible for inhibiting the DSB response, we used the *Xenopus* egg extract system, in which DSB checkpoint signaling can be reconstituted in vitro. This system allows easy manipulation of both DNA templates and Rsk signal components. Interphase extracts prepared from *Xenopus* eggs (crude S extracts) were treated with recombinant maltose-binding protein (MBP)-tagged Moloney sarcoma oncogene (Mos) kinase, a strong upstream activator of the MAPK pathway, leading to robust Rsk activation (38). This treatment markedly inhibited autophosphorylation of ATM induced by dsDNA without altering ATM levels. SL0101 treatment reversed this inhibition (Fig. 3*A*). To rule out the possibility that signaling by other Mos-activated kinases might cause the inhibition of the DSB response, we treated crude S extracts with prephosphorylated constitutively activated Rsk, and observed a similar decrease in ATM autophosphorylation (Fig. 3*B*). Because ATM must be recruited to the site of DNA break by the MRN complexes before autophosphorylation and monomerization, we investigated the binding of ATM to dsDNA. We immobilized biotin-tagged dsDNA on avidin beads to mimic sites of dsDNA damage, incubated the beads with crude S extracts, and retrieved DNA bead-associated proteins. We observed a significant decrease in dsDNA-bound ATM after pretreatment of extracts with Mos, whereas binding of another DNA damage-response protein, Ku70, was unchanged (Fig. 3*C*). To rule out the possibility that decreased ATM binding resulted from reduced ATM activity, we supplemented extracts with the ATM/ataxia telangiectasia and Rad3-related protein (ATR) kinase inhibitor caffeine; this supplementation did not reverse the decrease

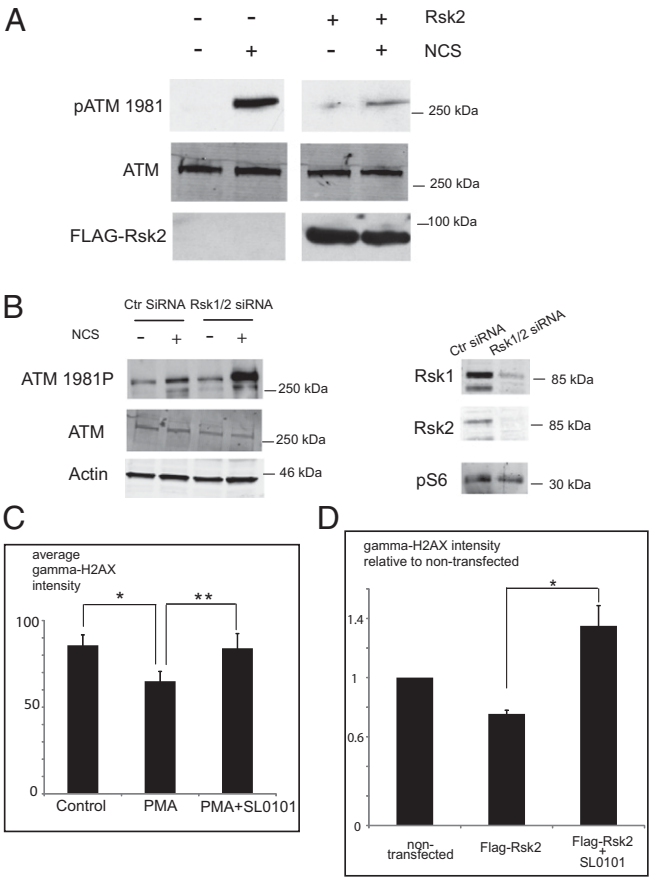

Fig. 2. Rsk suppresses the DSB response by inhibiting the activation of ATM. (*A*) HeLa cells transfected with FLAG-tagged Rsk2 were treated with NCS, lysed, and immunoblotted for phospho-ATM 1981. (*B*) Rsk1/2 knockdown PC3 cells were lysed and immunoblotted for phospho-ATM 1981. Cells treated with control siRNA were used as control. (*C*) HeLa cells grown on coverslips and treated with PMA ± SL0101 and then with NCS were fixed, stained, and examined for DAPI and γH2AX staining by fluorescence microscopy (20×). Average intensity of γH2ax staining from more than 50 cells from 10 random fields was quantified with MetaMorph. $*P < 0.01$; $**P < 0.01$. Error bars indicate SD. (*D*) HeLa cells, transfected with FLAG-tagged constitutively active Rsk2 were examined for γH2ax staining in FLAG-positive and -negative cells by fluorescence microscopy (40×). Average intensity of γH2ax staining from more than 40 FLAG-Rsk–positive and more than 300 FLAG-Rsk–negative cells from at least 18 random fields was quantified with MetaMorph. Fold change in intensity of γH2ax staining in FLAG-Rsk–positive relative to –negative cells was calculated. $*P < 0.01$. Error bars indicate SEM. Statistical analyses were done by the Student *t* test. Representative images from *C* and *D* are shown in Fig. S2 *C* and *D*, respectively.

in ATM/DNA binding (Fig. 3*D*). Together, these data suggest that Rsk functions upstream of ATM, affecting its recruitment to sites of DNA damage.

Because ATM recruitment is preceded by recognition of DNA-damage sites by the MRN complex, we investigated whether the binding of the MRN complex to dsDNA is affected by Rsk. Indeed, less Mre11 protein was associated with dsDNA in the crude S extracts pretreated with Mos than with control MBP protein. Moreover, SL0101 suppressed the effect of Mos (Fig. 3*D*). The association of Mre11 with the beads was DNA dependent; an excess of free DNA significantly decreased the levels of bead-bound Mre11 (Fig. S3*A*). Moreover, treatment with either the ATM inhibitor KU55933 or ATM/ATR inhibitor caffeine did not reverse Rsk's inhibition of Mre11 binding. This result strengthens the suggestion that the observed effect on MRN complex/DSB DNA assembly was not caused by feedback from downstream

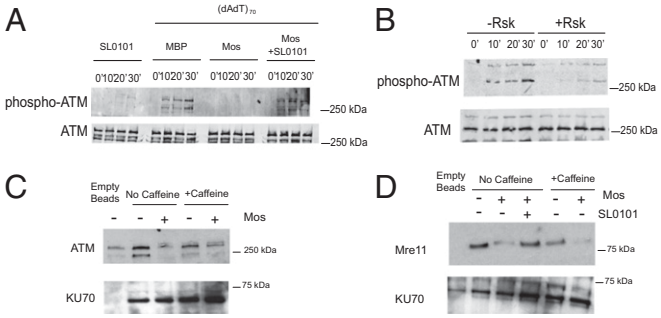

Fig. 3. The Mos/MAPK/Rsk pathway inhibits binding of the MRN complex to dsDNA. (*A*) *Xenopus* crude interphase extracts (S extracts) were treated with control MBP or MBP-Mos and then with SL0101 or DMSO, and double-stranded poly (dA-dT)$_{70}$. Samples were analyzed for ATM autophosphorylation by immunoblotting. (*B*) *Xenopus* crude S extracts were incubated with active RSK for 15 min before the addition of dsDNA. Samples were analyzed for ATM autophosphorylation by immunoblotting. (*C*) Crude S extracts were pretreated with MBP-Mos or MBP alone and caffeine and were incubated with biotin-tagged dsDNA-bound avidin beads. The amount of ATM bound to beads was analyzed by immunoblotting. DNA bound Ku70 was used as loading control. (*D*) *Xenopus* crude S extracts were pretreated with MBP-Mos or MBP ± caffeine or SL0101 and were incubated with biotin-tagged dsDNA which was bound to avidin beads. The amount of Mre11 protein bound to beads was analyzed by immunoblotting. Ku70 was the loading control.

ATM signaling (Fig. 3*D* and Fig. S3*A*). To confirm these findings in intact cells, we stained HeLa cells with anti-Mre11 antibody. PMA activation of Rsk significantly reduced the formation of Mre11/MRN foci, suggesting that Rsk indeed was suppressing the binding of the MRN complex to the DSB DNA (Fig. S3*B*).

To rule out the possibility that Rsk disrupts the interaction between Mre11 and other MRN complex components, we investigated binding of Mre11 to Nijmegen breakage syndrome 1 proteins (Nbs1) in egg extracts without added DNA. We did not observe any effect of Rsk on the phys-ical interaction between these two proteins (Fig. S3*C*), supporting the hypothesis that Rsk interferes with Mre11 binding to DNA but not with the formation of the MRN complex itself. To confirm that Rsk mediates suppression of ATM activation through the MRN complex, we treated cells with H_2O_2, which activates ATM independently of the MRN complex (39). Cells overexpressing Rsk displayed no change in ATM activation following H_2O_2 treatment, in agreement with our conclusion that Rsk silences ATM activation through suppression of MRN complex binding to DNA (Fig. S3*D*).

S676 on Mre11 is the Target of Rsk. To identify specific target(s) of Rsk, we isolated DNA-bound proteins from crude S egg extracts and incubated the precipitates with Rsk and radiolabeled ATP. The one major protein band identified by SDS/PAGE and autoradiography was ~85 kDa, which is the molecular weight of Mre11, suggesting that Mre11 might be a direct target of Rsk (Fig. S4*A*). This result was confirmed using His-tagged recombinant Mre11, which could be directly phosphorylated by Rsk2 kinase (Fig. 4*A*). To determine if the decreased MRN/dsDNA binding was cause by phosphorylation of Mre11, we prephosphorylated Mre11 with Rsk2 and then incubated Mre11 with crude S extracts for 15 min (to allow association of other required factors) before precipitating the dsDNA. As shown in Fig. 4*B*, prephosphorylation by Rsk2 reduced the binding of Mre11 to dsDNA, suggesting that phosphorylation of Mre11 contributes to Rsk-mediated inhibition of the DSB response. To identify the relevant sites of phosphorylation on Mre11, we phosphorylated recombinant His-tagged Mre11 with Rsk in vitro and analyzed the protein by mass spectrometry. We identified four phosphorylated residues: 2, 641, 676, and 688. Although none of those four sites was identical to the Rsk consensus site RXRXXpS/T, Rsk can target nonoptimal sites (40). We mutated each of the identified sites and performed in vitro Rsk assays using the recombinant mutants. Although several of the sites reduced phosphorylation, the single S676A mutation abolished phosphorylation almost completely, suggesting that S676 is the major site of in vitro phosphorylation by Rsk (Fig. 4*C*). Mre11 phosphorylation also was severely compromised by mutation of S676 when radiolabeled ATP was added to lysates that had been prepared from cells transfected with Rsk (Fig. S4*B*). Note that in this experiment, cells were not serum starved before lysate production, and thus WT or constitutively activated Rsk proteins behaved similarly (because of the activation of the transfected WT Rsk). As is consistent with our in vitro data, we successfully detected endogenous Mre11 S676 phosphorylation in the presence of PMA or overexpressed WT/constitutively active Rsk with an antibody that targeted phospho-S676 (Fig. 4 *D* and *E*). Phosphorylation induced by PMA was abrogated by cotreatment with the Rsk inhibitor SL0101 (Fig. 4 *D* and *E*). In addition, we treated Rsk-transfected cells with a DNA PK inhibitor to rule out the possibility that Rsk might cause Mre11 S676 phosphorylation indirectly by activating DNA PK (Fig. S5*A*). Although the DNA PK inhibitor was effective against a known DNA PK substrate, Akt, it did not inhibit phosphorylation of Mre11 downstream of Rsk (Fig. S5*B*). Collectively, these data suggested that Rsk can phosphorylate S676 of Mre11 both in vitro and in intact cells.

Phosphorylation of Mre11 on S676 Reduces Its Binding to dsDNA and Is Responsible for Checkpoint Inhibition by Rsk. Mre11 has two potential DBDs, and S676 is located within the second of these (Fig. 5*A*) (41, 42). Therefore, we speculate that phosphorylation of Mre11 on S676 might directly disrupt its binding to dsDNA. As shown in Fig. 5*B*, Mos treatment of egg extracts reduced binding of WT Mre11 to DNA beads but had no effect on the S676A mutant. Moreover, pretreating recombinant WT Mre11 with Rsk

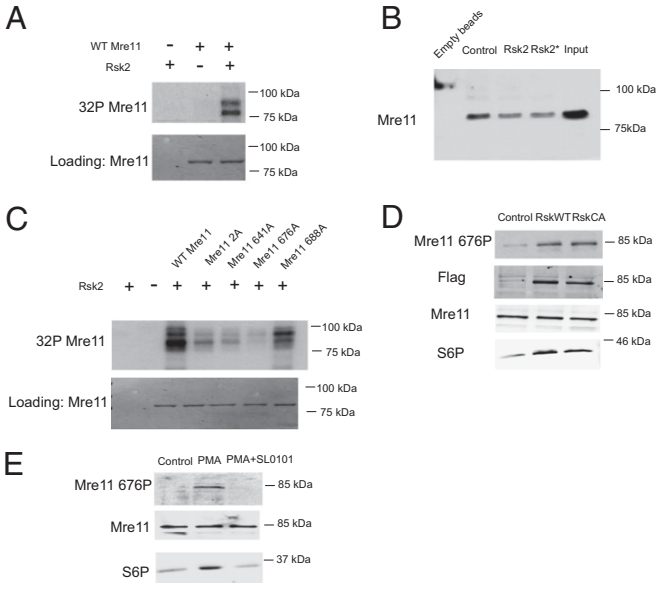

Fig. 4. Rsk phosphorylates Mre11 at S676. (*A*) Purified Mre11 protein was treated with Rsk and radiolabeled ATP (in kinase buffer), and labeled proteins were subjected to SDS/PAGE and autoradiography. (*B*) His-tagged Mre11 protein was phosphorylated in vitro using RSK kinase and added to *Xenopus* egg extracts for 10 min. Biotin-tagged dsDNA was used to pull down Mre11, and samples were analyzed for Mre11/dsDNA interaction by His-immunoblotting. In one sample (Rsk*), SL0101 and phosphatase inhibitors were added to extracts to prevent further phosphorylation by Rsk or dephosphorylation by phosphatases. (*C*) Equal amounts of His-tagged Mre11 protein and mutants were treated as in *A*. (*D*) Lysates from 293T cells transfected with WT or constitutively active (CA) Rsk were analyzed for endogenous S676 phosphorylated Mre11 by immunoblotting with phospho-specific antibody. (*E*) Lysates from 293T cells treated with PMA ± SL0101 were analyzed for endogenous S676 phosphorylated Mre11 by immunoblotting with phospho-specific antibody.

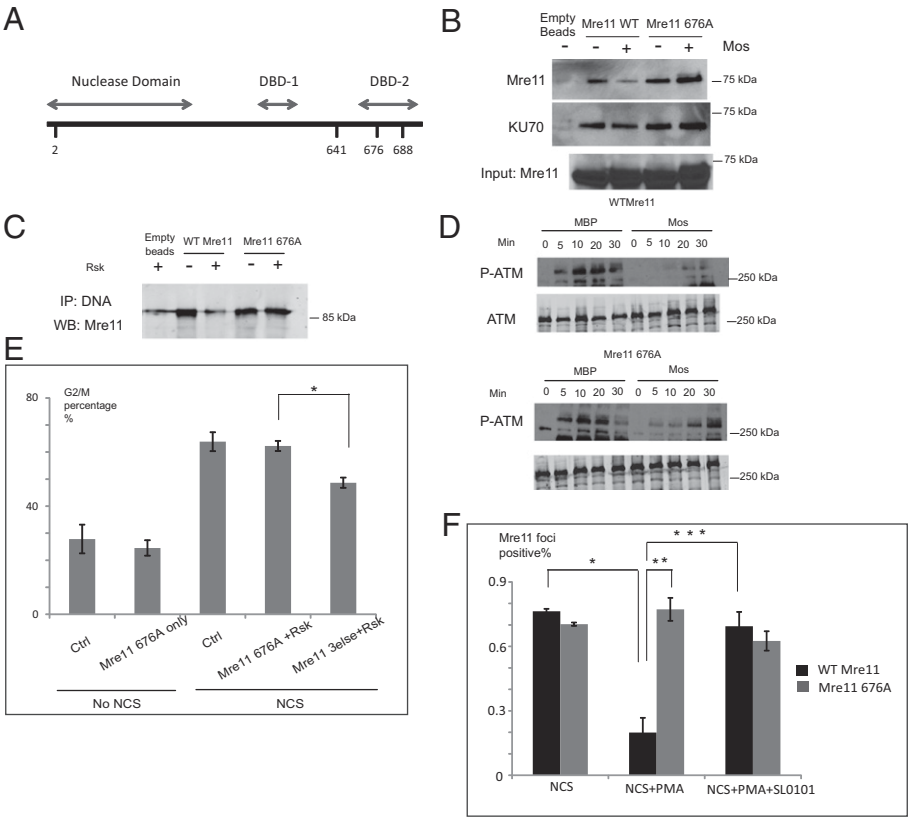

Fig. 5. Phosphorylation of Mre11 on S676 reduces its binding to DNA and reverts checkpoint inhibition. (*A*) Mre11 DNA-binding domains were within its C-terminal half. (*B*) *Xenopus* crude S extracts pretreated with MBP-Mos or MBP and supplemented with WT or mutant Mre11 proteins were incubated with biotin-tagged dsDNA-bound avidin beads. The amount of Mre11 protein bound to the beads was analyzed by immunoblotting. (*C*) WT or mutant Mre11 proteins pretreated with Rsk were incubated with biotin-tagged dsDNA-bound avidin beads in PBS buffer for 20 min. Samples were then processed as in *B*. (*D*) *Xenopus* crude S extracts with Mre11 WT or S676A proteins treated with MBP-Mos or MBP and then dsDNA were immunoblotted for phosphorylated ATM. (*E*) 293T cells transfected with FLAG-tagged constitutively active Rsk2 and HA-tagged Mre11 S676A or Mre11 mutated to A at S/T 2, 641, and 688 were stained with propidium iodide, anti-HA, and anti-FLAG antibody. DNA profiles of total and HA-positive/FLAG-positive populations were analyzed. $*P < 0.01$. Error bars indicate SD. (*F*) HeLa cells infected with Mre11 shRNA and transfected with shRNA-resistant WT Mre11 or the S676 mutant were treated with PMA and SL0101 and then with NCS. Fixed cells were stained with DAPI and anti-Mre11 antibody and were analyzed by fluorescence microscopy (40×). Representative images are shown in Fig. S6. Cells with more than five clear Mre11 foci were counted as Mre11-positive. The quantitation of more than 50 cells from at least eight random fields from each of three experiments is shown. $*P < 0.001$; $**P < 0.001$; $***P < 0.001$. Error bars indicate SD.

reduced the amount of DNA-bound Mre11, but this effect was not seen when the S676A mutant was used (Fig. 5*C*).

Consistent with the role for Mre11 S676 phosphorylation in the control of ATM by Rsk, we found that the ability of Mos to inhibit DSB-induced ATM activation in *Xenopus* egg extracts was dampened significantly by the addition of the S676A mutant Mre11 (Fig. 5*D*). Moreover, upon expression in 293T cells, the S676A mutant conferred resistance to Rsk-mediated G2/M checkpoint inhibition, whereas the control mutant (mutated at the other sites originally seen by mass spectrometry, 2A/641A/688A) did not (Fig. 5*E*). We further investigated whether Rsk directly inhibited the formation of Mre11/MRN foci in Mre11-mutant cells. We knocked down endogenous Mre11 in HeLa cells using shRNA and transfected cells with shRNA resistant WT Mre11 or S676A. PMA treatment reduced the Mre11 foci in cells expressing WT Mre11 but not in the cells expressing the S676A mutant (Fig. 5*F* and Fig. S6). Moreover, SL0101 reversed the effect of PMA in the WT-expressing cells, as is consistent with a role of Rsk in controlling the formation of Mre11/MRN foci via phosphorylation of Mre11 S676 (Fig. 5*F* and Fig. S6).

Discussion

We have shown here that Rsk signaling impairs cell-cycle arrest by the DSB-induced G2/M checkpoint by inhibiting the ATM pathway. This effect appears to involve a failure to activate ATM through MRN-mediated recruitment to sites of DNA damage. We found that Mre11 protein, a core constituent of the MRN complex, was phosphorylated by Rsk both in vitro and in intact cells. Furthermore, through mutagenesis experiments, one of the identified phosphorylation sites, S676, was demonstrated to be essential for functionally inhibiting Mre11. Together, these findings provide a mechanism for Rsk-induced inhibition of DSB checkpoint function.

A recent paper investigating the role of Rsk in G2/M arrest following doxorubicin treatment reported that Rsk could phosphorylate Chk1 at S280, the site that is targeted by Akt kinase to inhibit Chk1 activity (30). However, a similar study showed that the same phosphorylation on Chk1 had the opposite effect (31). Our findings are distinct from these reports in demonstrating that Rsk-mediated inhibition of ATM activation can be achieved by targeting steps upstream of ATM activation. In addition, Rsk can suppress G2/M checkpoint function following DSB in cells knocked down for Chk1, suggesting that Rsk phosphorylation of Mre11 contributes to DSB-induced G2 checkpoint silencing independently of Chk1 (Fig. S7*A*).

The finding that phosphorylation on Mre11 at S676 inhibited its binding to the DSB also is consistent with a previous report demonstrating that mutation of eight SQ/TQ sites on Mre11, including S676, undermined the negative feedback loop whereby ATM terminates the checkpoint response by inhibiting DNA binding by Mre11 (32). Our study strongly suggests that S676 is, at least in part, responsible for such inhibition and that S676 phosphorylation can prevent binding of Mre11 to dsDNA not only in *Xenopus* extracts but also in mammalian cells. In addition, we implicate Mre11 phosphorylation as a factor in a critical checkpoint inhibitory pathway that results from high ambient MAPK signaling in cancer cells. Interestingly, Di Virgilio et al. suggested that ATM is not the only kinase responsible for the phosphorylation of the observed eight SQ/TQ phospho-sites (32). Indeed, it is possible that Rsk not only participates in a checkpoint inhibitory pathway but also acts downstream of ATM in the pathway of feedback inhibition. In other words, it may be that ATM can inhibit Mre11 by activating Rsk. We note that the converse cannot be true—i.e., Rsk cannot activate ATM to phosphorylate Mre11—because ATM inhibition did not preclude Rsk-mediated phosphorylation or inhibition of Mre11.

The DNA-damage response and its regulation have been shown to play a critical role in tumorigenesis; the DSB-response pathway can be turned off early in tumor development in multiple types of cancer. This abrogation of checkpoint function prevents cell-cycle arrest, leads to error-prone DNA replication, and promotes accumulation of multiple cellular mutations (which can fuel cancer progression) (43, 44). Moreover, because the primary goal of radiation therapy is the generation of abundant DSBs to induce

permanent cell-cycle arrest and/or apoptosis, the overriding of DSB-induced checkpoint function can undermine the utility of this treatment modality. Indeed as shown in Fig. S7*B*, in the cells we tested, up-regulation of Rsk rendered cells resistant to excessive DSB-induced cell death. However, it should be noted that in some radioresistant tumors the DSB response and DNA repair are up-regulated rather than inactivated, leading to efficient repair of radiation-induced DNA damage (45). Consequently, the therapeutic benefit of inhibiting or activating the DSB response is likely to vary depending on tumor type. This variance has clear implications for Rsk as a target of tumor therapy. In cancer cells that inhibit their checkpoint function through Rsk, Rsk inhibition might be synergistic with ionizing radiation.

The consequences of inhibiting Rsk for cancer therapy extend beyond the impact on cell-cycle checkpoints and DNA repair. Recently, our laboratory reported that Rsk can phosphorylate the apoptotic inducer Apaf-1 and thereby reduce its apoptotic activity (21). Similarly, it has been reported that Rsk can inhibit the action of Bax/Bad complexes, a pivotal mediator of cell death following both chemotherapy and radiation (46). Therefore, at least for tumors with high Rsk activity, inhibition of Rsk may restore DNA damage-induced cell-cycle arrest while at the same time removing the brake on apoptosis. In these tumors, Rsk inhibitors may extend the utility of both irradiation and DNA-damaging chemotherapeutics.

Materials and Methods

Detailed information on materials and protocols is given in *SI Materials and Methods*.

***Xenopus* Extracts and DNA Immunoprecipitation.** Cytostatic factor (CSF) extracts and interphase extracts were prepared as previously described (38). Detailed information is provided in *SI Materials and Methods*.

Immunostaining. HeLa cells were grown on coverslips, were treated with different drugs as described in *Results*, and were fixed with 4% (vol/vol) paraformaldehyde for 20 min. Immunostaining was performed as described previously (47) using anti-γH2AX antibody.

ACKNOWLEDGMENTS. We thank John Blenis (Harvard Medical School) for providing the Rsk plasmids; William Dunphy (California Institute of Technology) for the Xenopus ATM and Nbs1 antibody; Bin Li (Duke Cancer Institute Flow Core Facility) for FACS analyses; Jiyeon Kim for Rsk siRNA and scientific advice; Denise Ribar, Wanli Tang, Manabu Kurokawa, Christopher Freel, and Stephanie Freel for technical assistance; and members of the S.K. laboratory for helpful discussions. This work was supported by National Institutes of Health Grants R01 GM080333 and CA102707 (to S.K.).

1. Agarwal S, Tafel AA, Kanaar R (2006) DNA double-strand break repair and chromosome translocations. *DNA Repair (Amst)* 5(9-10):1075–1081.
2. Lee JH, Paull TT (2004) Direct activation of the ATM protein kinase by the Mre11/Rad50/Nbs1 complex. *Science* 304(5667):93–96.
3. Abraham RT (2001) Cell cycle checkpoint signaling through the ATM and ATR kinases. *Genes Dev* 15(17):2177–2196.
4. Kim ST, Lim DS, Canman CE, Kastan MB (1999) Substrate specificities and identification of putative substrates of ATM kinase family members. *J Biol Chem* 274(53):37538–37543.
5. Kastan MB, Lim DS (2000) The many substrates and functions of ATM. *Nat Rev Mol Cell Biol* 1(3):179–186.
6. Matsuoka S, et al. (2000) Ataxia telangiectasia-mutated phosphorylates Chk2 in vivo and in vitro. *Proc Natl Acad Sci USA* 97(19):10389–10394.
7. Hawley RS, Friend SH (1996) Strange bedfellows in even stranger places: The role of ATM in meiotic cells, lymphocytes, tumors, and its functional links to p53. *Genes Dev* 10(19):2383–2388.
8. Jackson SP (2001) Detecting, signalling and repairing DNA double-strand breaks. *Biochem Soc Trans* 29(Pt 6):655–661.
9. Lavin MF (2007) ATM and the Mre11 complex combine to recognize and signal DNA double-strand breaks. *Oncogene* 26(56):7749–7758.
10. Smith JA, Poteet-Smith CE, Malarkey K, Sturgill TW (1999) Identification of an extracellular signal-regulated kinase (ERK) docking site in ribosomal S6 kinase, a sequence critical for activation by ERK in vivo. *J Biol Chem* 274(5):2893–2898.
11. Dalby KN, Morrice N, Caudwell FB, Avruch J, Cohen P (1998) Identification of regulatory phosphorylation sites in mitogen-activated protein kinase (MAPK)-activated protein kinase-1a/p90rsk that are inducible by MAPK. *J Biol Chem* 273(3):1496–1505.
12. Sturgill TW, Ray LB, Erikson E, Maller JL (1988) Insulin-stimulated MAP-2 kinase phosphorylates and activates ribosomal protein S6 kinase II. *Nature* 334(6184):715–718.
13. Zhao Y, Bjørbaek C, Weremowicz S, Morton CC, Moller DE (1995) RSK3 encodes a novel pp90rsk isoform with a unique N-terminal sequence: Growth factor-stimulated kinase function and nuclear translocation. *Mol Cell Biol* 15(8):4353–4363.
14. Bunone G, Briand PA, Miksicek RJ, Picard D (1996) Activation of the unliganded estrogen receptor by EGF involves the MAP kinase pathway and direct phosphorylation. *EMBO J* 15(9):2174–2183.
15. De Cesare D, Jacquot S, Hanauer A, Sassone-Corsi P (1998) Rsk-2 activity is necessary for epidermal growth factor-induced phosphorylation of CREB protein and transcription of c-fos gene. *Proc Natl Acad Sci USA* 95(21):12202–12207.
16. Grove JR, et al. (1993) Regulation of an epitope-tagged recombinant Rsk-1 S6 kinase by phorbol ester and erk/MAP kinase. *Biochemistry* 32(30):7727–7738.
17. Ryves WJ, Evans AT, Olivier AR, Parker PJ, Evans FJ (1991) Activation of the PKC-isotypes alpha, beta 1, gamma, delta and epsilon by phorbol esters of different biological activities. *FEBS Lett* 288(1-2):5–9.
18. Smith JA, et al. (2005) Identification of the first specific inhibitor of p90 ribosomal S6 kinase (RSK) reveals an unexpected role for RSK in cancer cell proliferation. *Cancer Res* 65(3):1027–1034.
19. Clark DE, et al. (2005) The serine/threonine protein kinase, p90 ribosomal S6 kinase, is an important regulator of prostate cancer cell proliferation. *Cancer Res* 65(8):3108–3116.
20. Xian W, et al. (2009) Fibroblast growth factor receptor 1-transformed mammary epithelial cells are dependent on RSK activity for growth and survival. *Cancer Res* 69(6):2244–2251.
21. Kim J, et al. (2012) Rsk-mediated phosphorylation and 14-3-3ε binding of Apaf-1 suppresses cytochrome c-induced apoptosis. *EMBO J* 31(5):1279–1292.
22. Lee YJ, et al. (2002) Protein kinase Cdelta overexpression enhances radiation sensitivity via extracellular regulated protein kinase 1/2 activation, abolishing the radiation-induced G(2)-M arrest. *Cell Growth Differ* 13(5):237–246.
23. Warenius HM, et al. (2000) Combined RAF1 protein expression and p53 mutational status provides a strong predictor of cellular radiosensitivity. *Br J Cancer* 83(8):1084–1095.
24. Rinehart J, et al. (2004) Multicenter phase II study of the oral MEK inhibitor, CI-1040, in patients with advanced non-small-cell lung, breast, colon, and pancreatic cancer. *J Clin Oncol* 22(22):4456–4462.
25. Sebolt-Leopold JS, Herrera R (2004) Targeting the mitogen-activated protein kinase cascade to treat cancer. *Nat Rev Cancer* 4(12):937–947.
26. Sebolt-Leopold JS (2004) MEK inhibitors: A therapeutic approach to targeting the Ras-MAP kinase pathway in tumors. *Curr Pharm Des* 10(16):1907–1914.
27. Eisinger-Mathason TS, Andrade J, Lannigan DA (2010) RSK in tumorigenesis: Connections to steroid signaling. *Steroids* 75(3):191–202.
28. Sapkota GP, et al. (2007) BI-D1870 is a specific inhibitor of the p90 RSK (ribosomal S6 kinase) isoforms in vitro and in vivo. *Biochem J* 401(1):29–38.
29. Cohen MS, Zhang C, Shokat KM, Taunton J (2005) Structural bioinformatics-based design of selective, irreversible kinase inhibitors. *Science* 308(5726):1318–1321.
30. Ray-David H, et al. (2013) RSK promotes G2 DNA damage checkpoint silencing and participates in melanoma chemoresistance. *Oncogene* 32(38):4480–4489.
31. Li P, et al. (2012) P90 RSK arranges Chk1 in the nucleus for monitoring of genomic integrity during cell proliferation. *Mol Biol Cell* 23(8):1582–1592.
32. Di Virgilio M, Ying CY, Gautier J (2009) PIKK-dependent phosphorylation of Mre11 induces MRN complex inactivation by disassembly from chromatin. *DNA Repair (Amst)* 8(11):1311–1320.
33. Xu B, Kim ST, Lim DS, Kastan MB (2002) Two molecularly distinct G(2)/M checkpoints are induced by ionizing irradiation. *Mol Cell Biol* 22(4):1049–1059.
34. Zhou BB, et al. (2000) Caffeine abolishes the mammalian G(2)/M DNA damage checkpoint by inhibiting ataxia-telangiectasia-mutated kinase activity. *J Biol Chem* 275(14):10342–10348.
35. Wang Y, et al. (2012) Berberine, a genotoxic alkaloid, induces ATM-Chk1 mediated G2 arrest in prostate cancer cells. *Mutat Res* 734(1-2):20–29.
36. Kumareswaran R, et al. (2012) Chronic hypoxia compromises repair of DNA double-strand breaks to drive genetic instability. *J Cell Sci* 125(Pt 1):189–199.
37. Laval A, Kao J, Peters S (2007) ATM phosphorylation kinetics as a biological reporter of cellular radiosensitivity. *Int J Radiat Oncol* 69(3):S65–S66.
38. Wu JQ, et al. (2007) Control of Emi2 activity and stability through Mos-mediated recruitment of PP2A. *Proc Natl Acad Sci USA* 104(42):16564–16569.
39. Guo Z, Deshpande R, Paull TT (2010) ATM activation in the presence of oxidative stress. *Cell Cycle* 9(24):4805–4811.
40. Buck M, Poli V, Hunter T, Chojkier M (2001) C/EBPbeta phosphorylation by RSK creates a functional XEXD caspase inhibitory box critical for cell survival. *Mol Cell* 8(4):807–816.
41. Stracker TH, Theunissen JW, Morales M, Petrini JH (2004) The Mre11 complex and the metabolism of chromosome breaks: The importance of communicating and holding things together. *DNA Repair (Amst)* 3(8-9):845–854.
42. Paull TT, Gellert M (2000) A mechanistic basis for Mre11-directed DNA joining at microhomologies. *Proc Natl Acad Sci USA* 97(12):6409–6414.
43. Löbrich M, Jeggo PA (2007) The impact of a negligent G2/M checkpoint on genomic instability and cancer induction. *Nat Rev Cancer* 7(11):861–869.
44. Jackson SP, Bartek J (2009) The DNA-damage response in human biology and disease. *Nature* 461(7267):1071–1078.
45. Sakata K, Someya M, Matsumoto Y, Hareyama M (2007) Ability to repair DNA double-strand breaks related to cancer susceptibility and radiosensitivity. *Radiat Med* 25(9):433–438.
46. Hurbin A, et al. (2005) Cooperation of amphiregulin and insulin-like growth factor-1 inhibits Bax- and Bad-mediated apoptosis via a protein kinase C-dependent pathway in non-small cell lung cancer cells. *J Biol Chem* 280(20):19757–19767.
47. Zhang L, Huang NJ, Chen C, Tang W, Kornbluth S (2012) Ubiquitylation of p53 by the APC/C inhibitor Trim39. *Proc Natl Acad Sci USA* 109(51):20931–20936.

Supporting Information

Chen et al. 10.1073/pnas.1306328110

SI Materials and Methods

Xenopus Extracts and DNA Immunoprecipitation. For extracts treated with DSB DNA, 5 μL of 0.01 mM dAdT dsDNA (70 nt) was added to 50-μL extracts. Extracts were incubated at room temperature. For DNA precipitations, 1 μL of biotin-tagged dsDNA (0.25 mM) was bound to 25 μL of avidin beads for each reaction. DNA-bound beads then were incubated with 100-μL extracts for 20 min at room temperature. Beads were removed from extracts and washed four times with egg lysis buffer (250 mM sucrose, 2.5 mM MgCl, 1 mM DTT, 50 mM KCl, and 10 mM Hepes, pH 7.7).

Cell Culture and Drug Treatments. 293T, HeLa, or MCF7 cells were maintained in high-glucose DMEM medium supplemented with 10% FBS. PC3 cells were maintained in F12K medium. Cells were grown to 90% confluence before treatment with drugs. For SL0101 treatment, 1 μL of 100 mM SL0101 was added to 1 mL of medium for a final concentration of 100 uM. Cells were treated with SL0101 for 30 min. For phorbol12-myristate13-acetate (PMA) treatment, 0.5 μL of PMA (50 ng/μL) was added to 1 mL of medium to make final a concentration of 25 ng/mL Cells were treated for 30 min. For neocarzinostatin (NCS) treatment, 0.2 μL of NCS (500 ng/mL) was added to 1 mL medium to make a final concentration of 200 ng/mL After treatment for 30 min, cells were washed once with PBS.

Transfection and siRNA. FuGENE 6 (Roche) was used to transfect cells with plasmids according to the manufacturer's instructions. Lipofectamine RNAiMAX (Invitrogen) was used to perform siRNA transfections. siRNA targeted against ribosomal s6 kinase 1 (RSK1) and RSK2 as previously described (40) were purchased from Sigma.

Plasmid Reagents and Antibodies. C-terminal HA-tagged meiotic recombination 11 (Mre11) and N-terminal Flag-tagged RSK2 were cloned into pCDNA3 plasmid. Mre11 alanine mutants and the constitutively active RSK2 707A mutant were generated by site-directed mutagenesis. The antibodies against human Mre11 (Abcam), phospho-S6 Ser235/236 (Cell Signaling), phosphor-histone H3 (Ser10) (Cell Signaling), actin (Santa Cruz), phosphor-Mre11 Ser-676 (Cell Signaling), goat anti-HA (Abcam), His-probe (Santa Cruz), γH2AX Ser139 (Cell Signaling), human ataxia telangiectasia mutant (ATM) (Abcam), phospho-ATM Ser1981 (Epitomics), and anti-human/*Xenopus* Mre11 (Calbiochem) were obtained as stated.

The antibodies against *Xenopus* Nijmegen breakage syndrome 1 (Nbs1) and ATM were gifts from William Dunphy (California Institute of Technology, Pasadena, CA).

The following drugs were used: PMA (Enzo Life Science), NCS (Sigma), SL0101 (Calbiochem), and Ku55933 (Calbiochem).

Biotin-tagged ssDNA was purchased from Integrated DNA Technologies. Biotin-tagged dsDNA was synthesized by annealing tagged ssDNA with its anti-sense DNA at 70 °C and gradual cooling to room temperature.

Kinase Assay. For kinase assays in mammalian cell lysates, nickel-agarose–bound Mre11-His was incubated with 2 μCi γ-[^{32}P]ATP in cytosolic lysates from mammalian cells transfected with RSK2 for 1 h at 30 °C. Beads then were removed and washed three times in washing buffer [1 mM Hepes-KOH (pH 7.5), 1 mM β-glycerophosphate, 15 mM KCl, 0.1% Nonidet P-40, 14.8 mM imidazole, 500 mM NaCl, 1 mM $NaVO_3$, and 5 μg/mL aprotinin/leupeptin].

For the in vitro kinase assay, nickel-agarose–bound Mre11-His protein was incubated in kinase buffer [10 mM Tris·HCl (pH 7.5), 0.1 mM ATP, 10 mM $MgCl_2$, 1 mM DTT (pH 7.2)] with 2 μCiγ-[^{32}P]ATP and RSK2 kinase (Millipore). After 30 min at 30 °C, the beads were washed with washing buffer. Analysis for all kinase assays was performed using SDS/PAGE and autoradiography.

Immunoblot Analysis. For tissue culture, cells were cultured to 90% confluence before harvesting with trypsin. Cells then were lysed with extraction buffer [20 mM Hepes (pH 7.4), 150 mM NaCl, 12.5 mM M glycerophosphate, 1.5 mM $MgCl_2$, 2 mM EGTA, 10 mM NaF, 2 mM DTT, 1 mM Na_3VO_4, 20 μM aprotinin, 1 mM PMSF, and 0.5% Triton X-100]. The concentration of cell lysates was measured. Equal amounts of lysates were loaded for SDS/PAGE. Proteins were transferred from gels to PVDF membrane and were immunoblotted with antibodies. For large-molecular-weight proteins such as ATM, low-voltage (50 V) was used in the overnight transfer.

For *Xenopus* extracts, 5 μL of extract was mixed with 50 μL SDS sample buffer. Extracts and samples were loaded for SDS/PAGE, transferred from gels to PVDF membrane, and processed for immunoblotting with antibodies.

FACS. 293T cells were treated with inhibitors as describe in *Results* in the main text and after 22 h were fixed with 4% paraformaldehyde for 20 min. Cells then were permeabilized with 0.2% Triton in PBS buffer. After washing, cells were incubated with primary antibodies at 37 °C for 2 h and then with secondary antibody for 45 min. Cells were washed with PBS, treated with RNase for 15 min, and stained with propidium iodide (PI). Cell profiles were analyzed by flow cytometry. Each experiment was repeated three times, and the Student *t* test was applied to assess statistical significance. Significance levels are indicated in *Results* and figure legends.

Additional Information for Microscopy. For microscopy, a Zeiss Axio Imager widefield fluorescence microscope equipped with a mercury arc lamp (Zeiss HBO100 power supply and lamp housing) was used. The filter cube sets were Chroma 31000v2 (excitation wavelength range: 325 nm–375 nm, beam splitter: 410 nm, emission wavelength range: 435 nm–485 nm) for DAPI; Chroma 41017 (excitation wavelength range: 450 nm–490 nm, beam splitter Q495LP, emission wavelength range: 500 nm–550 nm) for GFP; and Chroma 41004 (excitation wavelength range: 535 nm–585 nm, beam splitter 595 nm: emission wavelength range, 610 nm–680 nm) for RFP. Objectives used were a Zeiss 20×/0.50 EC Plan-NeoFluar and a Zeiss 40×/0.75 EC Plan-NeoFluar. The camera was a Hamamatsu Orca ER monochrome cooled-CCD camera. The acquisition software was MetaMorph Premier version 7.7.3.0. Fluorescent intensity in the original raw images was quantified with MetaMorph. Blank areas within images were selected as background during quantification. Images also were adjusted for contrast and pseudocolored in MetaMorph for presentation in figures.

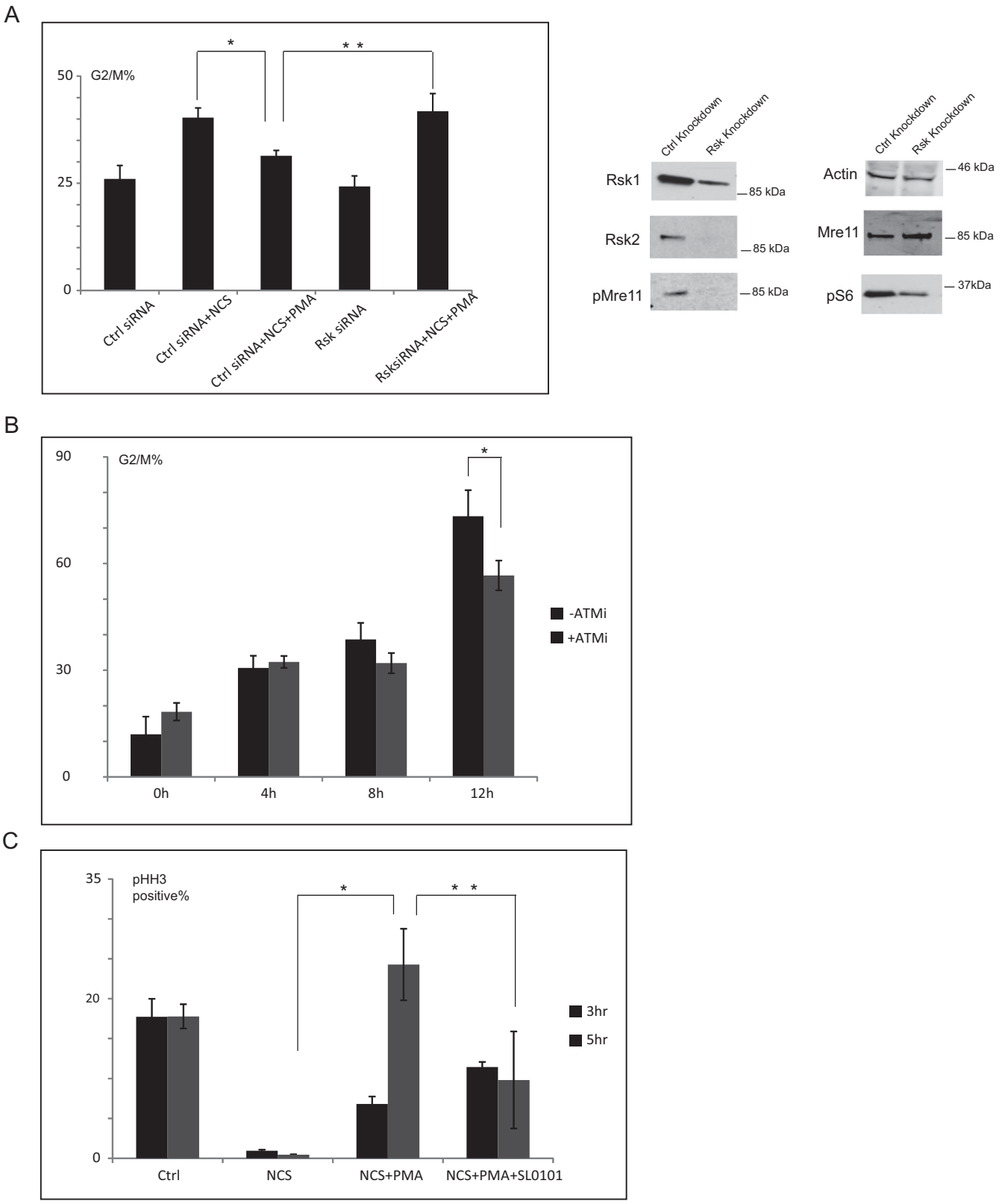

Fig. S1. (*A*) 293T cells were transfected with RSK1/2 siRNA. Forty-eight hours later, cells were treated with PMA for 30 min and then with NCS for another 30 min. (*Left*) Cells were collected after 16 h, and DNA profiles were analyzed by flow cytometry. (*Right*) The effectiveness of knockdown was analyzed by Western blotting. Data from three experiments were combined. $*P < 0.01$; $**P < 0.01$. Error bars indicate SD. (*B*) HeLa cells were treated with ATM inhibitor for 30 min and then with NCS for another 30 min. Cells were collected at the indicated time points, and DNA profiles were analyzed by flow cytometry. Data from three experiments were combined. $*P < 0.01$. Error bars indicate SD. (*C*) HeLa cells were synchronized in G1/S phase by double thymidine block. Four hours after release, cells were treated with PMA or SL0101 for 30 min and then with NCS for another 30 min. Three or five hours later cells were collected and stained

Legend continued on following page

with anti–phospho-Histone H3 antibody (pHH3). The pHH3-positive cells were analyzed by flow cytometry. Data from three experiments were combined. *$P <$ 0.001; **$P < 0.01$. Error bars indicate SD.

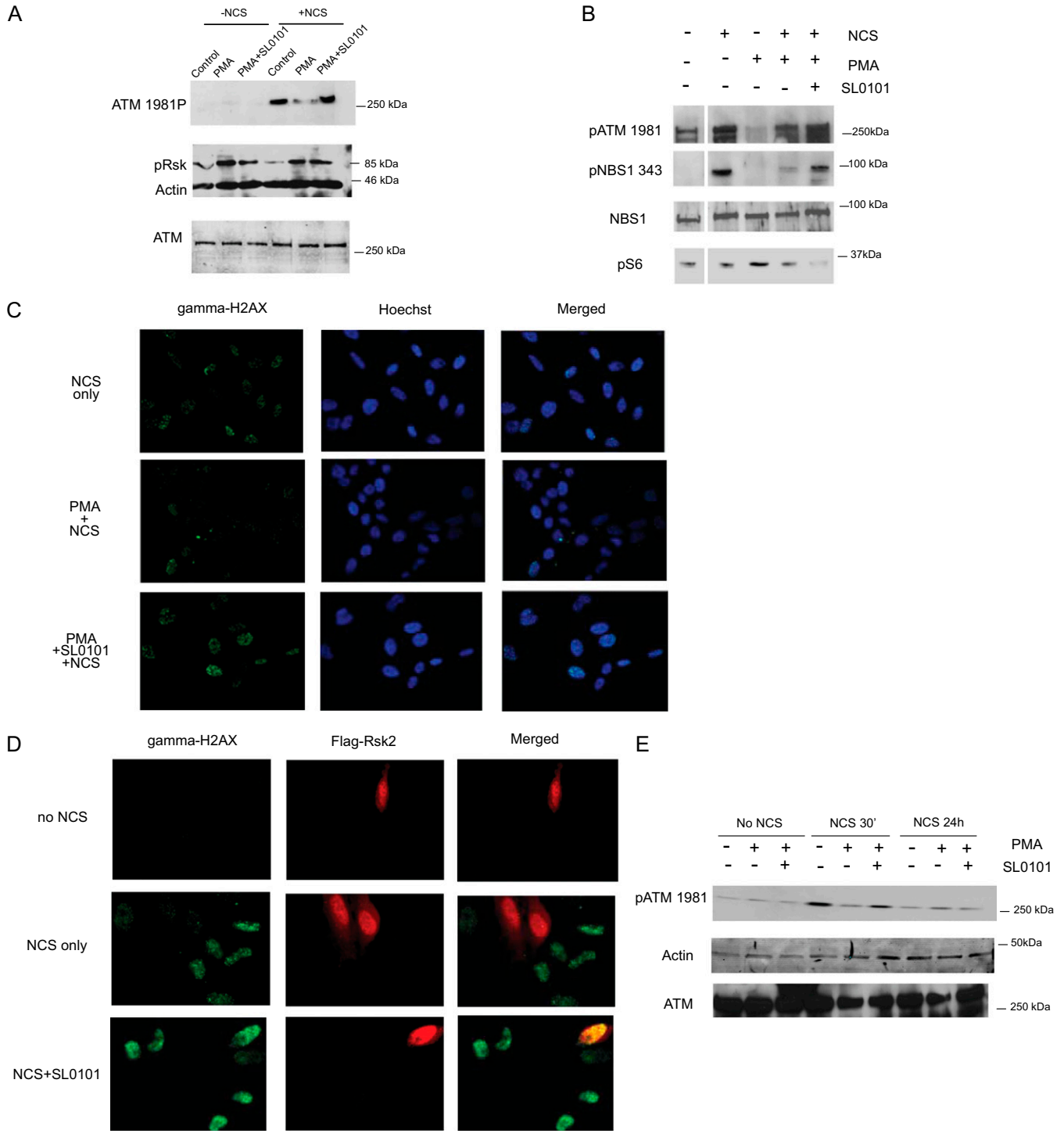

Fig. S2. (*A*) 293T cells were treated with PMA and SL0101 or with PMA alone for 30 min and then with NCS for another 30 min before harvesting. Cell lysates were immunoblotted for phospho-ATM 1981. (*B*) HeLa cells were treated with PMA or SL0101 for 30 min and then with NCS for another 30 min before harvesting. Cell lysates were immunoblotted for phospho-NBS1 Ser-343 and for phospho-ATM. (*C*) HeLa cells were stained with DAPI and rabbit anti-γH2AX. The pattern of γH2AX staining was examined by fluorescence microscopy. Images were taken under a 20× objective. (*D*) HeLa cells were transfected with FLAG-tagged constitutively active RSK2 and costained with mouse anti-FLAG and rabbit anti-γH2AX antibody. The pattern of γH2ax staining in FLAG-positive and -negative cells was examined by fluorescence microscopy. Images were taken under a 40× objective. (*E*) HeLa cells were treated with PMA or SL0101 for 30 min and then with NCS for another 30 min. Cells were harvested immediately or were cultured in regular medium for another 24 h before harvesting. Cell lysates were immunoblotted for phospho-ATM 1981.

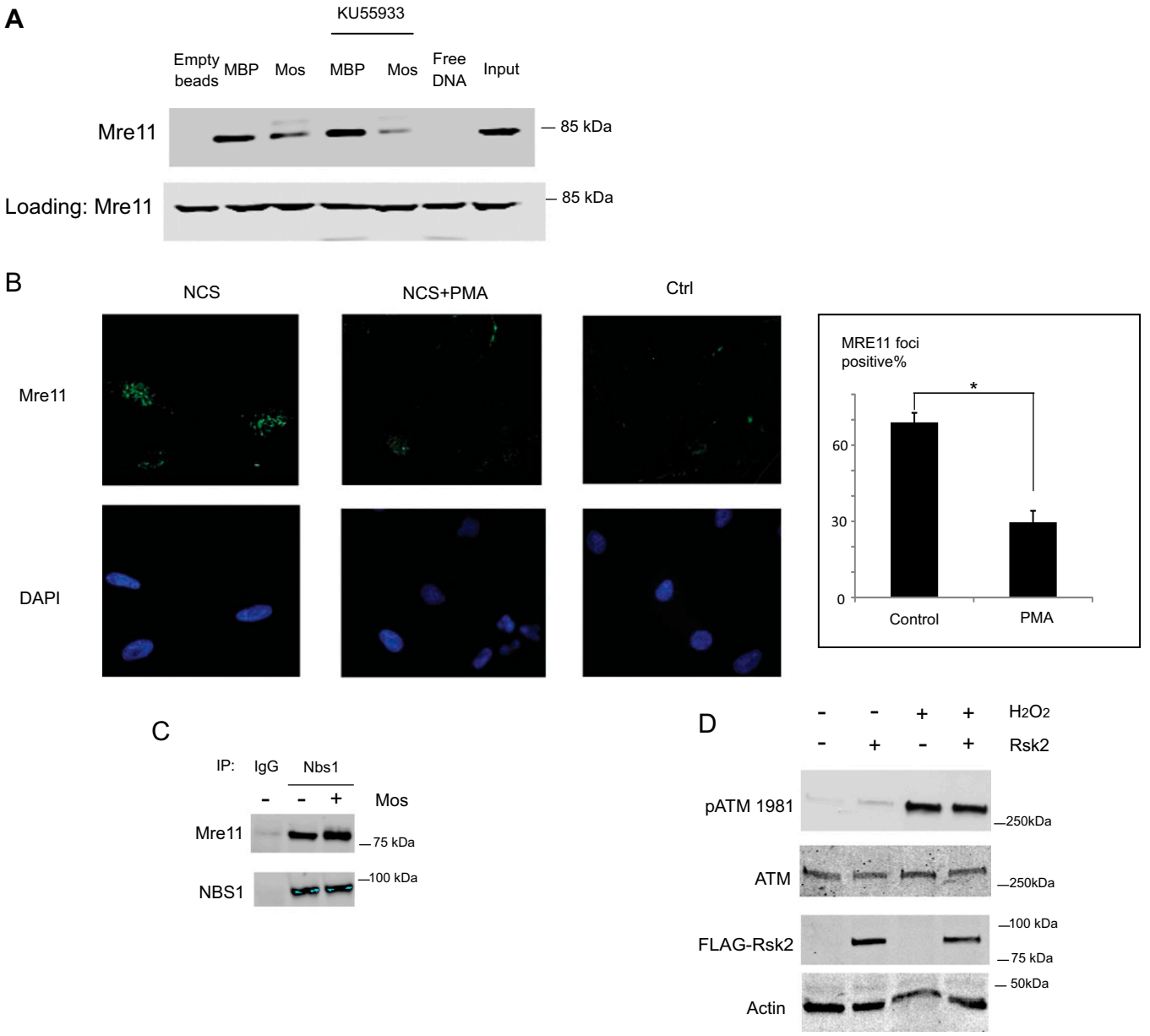

Fig. S3. (*A*) Biotin-tagged dsDNA was bound to avidin beads and added to *Xenopus* crude S extracts pretreated with maltose-binding protein (MBP)-Mos or with MBP and then KU55933 and were incubated for 20 min. In one of the reactions, free dsDNA was added to compete with the DNA on the beads. The amount of Mre11 protein bound to beads was analyzed by immunoblotting. (*B*) HeLa cells were grown on coverslips and were treated with PMA for 30 min and then with NCS for another 10 min before fixation. (*Left*) Cells were stained with DAPI and rabbit anti-Mre11. The pattern of Mre11 foci staining was examined by fluorescence microscopy. Images were taken under a 40× objective. Cells with more than five clear Mre11 foci were counted as Mre11-positive. (*Right*) Results from three experiments were combined. Fifty cells from at least 10 random fields were counted in each experiment. $*P < 0.001$. Error bas indicate SD. (*C*) Nbs1 protein was immunoprecipitated from *Xenopus* extract pretreated with Mos or MBP. Mre11 protein bound to Nbs1 was immunoblotted. (*D*) HeLa cells transfected with FLAG-tagged Rsk2 were treated with 0.9 mM H_2O_2 for 30 min before harvesting. Cell lysates were immunoblotted for phospho-ATM 1981.

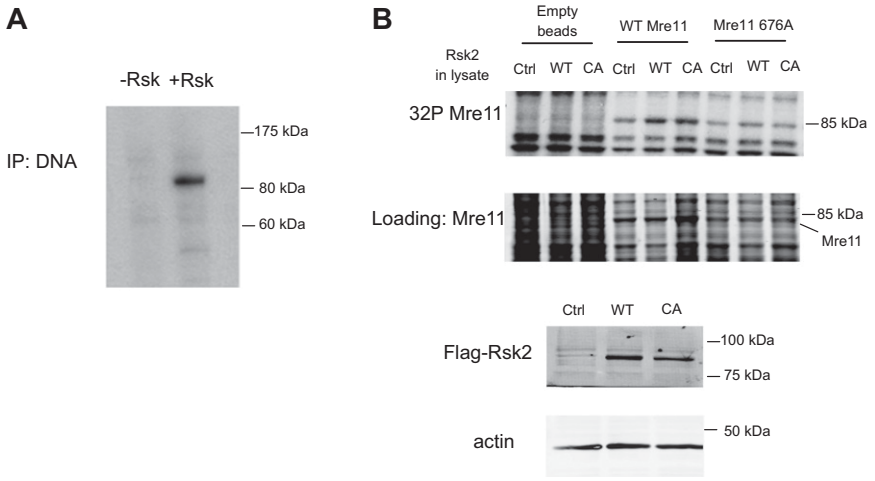

Fig. S4. (*A*) Biotin tagged-dsDNA was bound to avidin beads and incubated with *Xenopus* crude interphase egg extract for 20 min. After washing with egg lysis buffer, beads were spilt and treated with RSK2 kinase and γ-[^{32}P]ATP or with γ-[^{32}P]ATP alone as a control. Proteins were resolved in SDS sample buffer and analyzed by autoradiography. (*B*) 293T cells were transfected with WT Rsk or constitutively active Rsk (RSK CA). Cells were collected 2 d after transfection to make lysates. Equal amounts of WT His-tagged Mre11 protein and the 676A mutant proteins were mixed with lysates, kinase buffer, and γ-[^{32}P]ATP at 37 °C for 45 min. Radiolabeled Mre11 protein was analyzed by autoradiography.

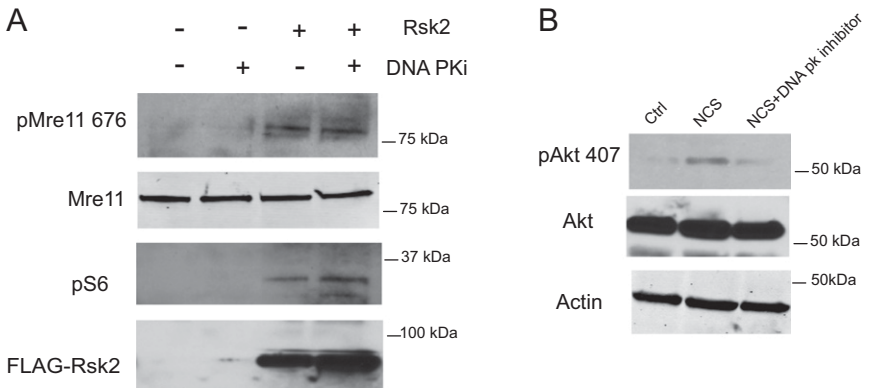

Fig. S5. (*A*) HeLa cells transfected with active Rsk2 kinase were treated with DNA PKC inhibitor for 30 min before harvesting. Lysates were blotted for anti-Mre11 Ser-676 antibody. (*B*) HeLa cells were treated with DNA PKC inhibitor for 30 min and then with NCS for another 30 min before harvesting. Lysates were immunoblotted with anti-Akt Ser407 antibody to see whether phosphorylation of Akt by DNA PKc was inhibited.

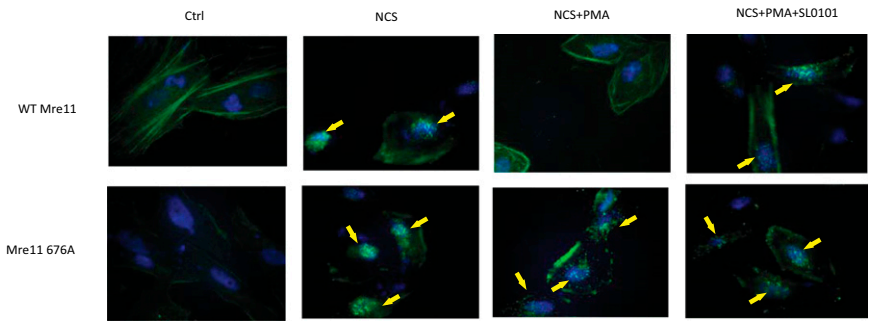

Fig. S6. HeLa cells infected with Mre11 shRNA were grown on coverslips and transfected with shRNA-resistant WT Mre11 or 676A mutant. Forty-eight hours after transfection, cells were treated with PMA and SL0101 for 30 min and then with NCS for another 10 min before fixation. Cells were stained with DAPI and rabbit anti-Mre11 antibody. The pattern of Mre11 foci staining was examined by fluorescence microscopy. Images were taken under a 40× objective. Shown are representative images of more than 50 cells from at least eight random fields from three experiments.(See Fig. 5*F* for quantitation.) Yellow arrows indicate Mre11 foci in the nuclei.

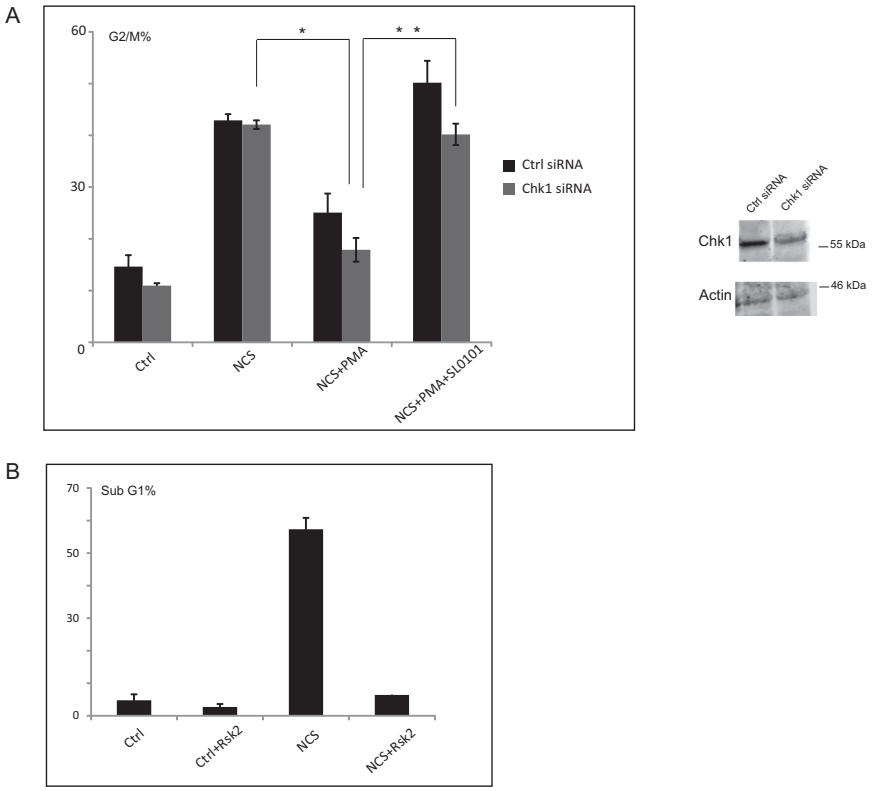

Fig. S7. (*A*) 293T cells were treated with siRNA to knock down endogenous checkpoint kinase 1 (Chk1). Forty-eight hours later, cells were treated with PMA and/or SL0101 for 30 min and then with NCS for another 30 min. Cells were grown in DMEM medium for 16 h before harvesting, and DNA profiles were analyzed by flow cytometry. Data from three experiments were combined. $*P < 0.01$. Error bars indicate SD. Note that the knockdown of Chk1 had minimal effect on the response to NCS, possibly because the ATM/Chk2 pathway, the primary pathway for the dsDNA-break response, remained intact. (*B*) HeLa cells were transfected with constitutively active Rsk2 kinase. After 36 h, cells were treated with 200 ng/mL NCS for 1 h. Cells were grown in DMEM medium for another 48 h before harvesting. DNA profiles were analyzed by flow cytometry, and the sub-G1 population was analyzed. Data from three experiments were combined. Error bars indicate SD.